



# A case study of seismic forward prospecting based on the tunnel seismic while drilling and active seismic methods

Xinji Xu<sup>1</sup> · Panlong Zhang<sup>2</sup> · Xu Guo<sup>1</sup> · Bin Liu<sup>1,2,3</sup> · Lei Chen<sup>1,2,4</sup> · Qingsong Zhang<sup>1</sup> · Lichao Nie<sup>1</sup> · Yi Zhang<sup>2</sup>

Received: 22 June 2019 / Accepted: 17 December 2020 / Published online: 9 March 2021  
© Springer-Verlag GmbH Germany, part of Springer Nature 2021

## Abstract

Forward prospecting to predict the location of high-risk geological zones during tunnel boring machine (TBM) tunneling is important for safe and efficient tunnel construction. Seismic forward-prospecting methods are sensitive to geological structures and have been widely used in areas with relatively well-developed structures, such as mountainous areas with active tectonics. The Gaoligongshan Tunnel in Yunnan, China, with an advance pilot tunnel, was chosen for this study. The advantages of seismic while tunneling and active source methods for different detection distances were investigated, and the methods were combined to determine the geological conditions. An excavate geological study of the tunnel had identified fractured zones ahead of the tunnel face. Our seismic prospecting results were basically consistent with this conclusion. On the basis of these data, the excavation rate was slowed and tunnel support was increased; excavation through the area was then able to proceed without incident. The presence of a pilot tunnel was found to create interference in the seismic signals. We modeled this effect with numerical simulations. On the basis of the results, we discuss appropriate observation systems for use in tunneling projects with pilot tunnels. We demonstrate that seismic signals received by geophones coupled to the wall further from the pilot tunnel reflected the geological conditions for both seismic while tunneling and active source methods. The seismic source should thus be placed on the tunnel wall further from the pilot tunnel to improve results.

**Keywords** Tunnel seismic while drilling (TSWD) · Active seismic method · Observation system · Fracture zone · Gaoligongshan tunnel

## Introduction

The rapid development of infrastructure has created the demand for a large number of tunnels to meet the needs of industries such as mining, transportation, and energy transport. Tunnel engineering thus plays a significant role in these fields. Tunnel boring

machines (TBMs) are widely used because they are faster and safer than traditional drilling and blasting methods (Yin et al. 2005), thus facilitating efficient and economic tunnel construction (Petronio and Poletto 2002).

However, TBMs can struggle to adapt to adverse geological conditions, sometimes resulting in serious accidents

✉ Bin Liu  
liubin0635@163.com

✉ Lichao Nie  
lichaojie@163.com

Xinji Xu  
xuxinji1990@163.com

Panlong Zhang  
zhangpl2019@163.com

Xu Guo  
guoxu1014@163.com

Lei Chen  
clei667@163.com

Qingsong Zhang  
zhangqingsong@sdu.edu.cn

Yi Zhang  
zy15522208076@163.com

<sup>1</sup> Geotechnical and Structural Engineering Research Center, Shandong University, 17923 Jingshi Road, Jinan 250061, China

<sup>2</sup> School of Qilu Transportation, Shandong University, Jinan 250061, China

<sup>3</sup> Data Science Institute, Shandong University, Jinan 250061, China

<sup>4</sup> Department of Civil and Environmental Engineering, University of Connecticut, Storrs, CT 06269-3037, USA

(Parise et al. 2008). Sudden malfunctions such as machine blockage, tunnel collapse, and water or mud inrush can result in substantial losses (Yin et al. 2005). For example, there were several incidents of water and mud inrush during tunneling at the Dul Hasti Hydroelectric Project in India and, as a result, it led to schedule delays (Vibert et al. 2005). While drilling the Pinglin Tunnel, a TBM became blocked while passing through a wide fractured zone early in the project (Barton 2012). Several machine blockage accidents caused a major 300-day delay during the construction of the Shanggongshan Tunnel in the Yunnan Province of China, and the TBM was ultimately abandoned in favor of drilling and blasting (Tiantian et al. 2004). It is thus important for geotechnical engineers to focus on avoiding such incidents.

Forward prospecting methods are of interest in tunnel engineering because they can detect geological conditions ahead of the tunnel face, allowing necessary support measures to be taken (Price 2008; Chen et al. 2011; Jiao et al. 2015; Yokota et al. 2016; Li et al. 2017). At present, the forward prospecting methods used for TBM tunnels include advanced drilling surveys, advance pilot tunneling, and non-destructive geophysical investigations (Zhang and Fu 2007). The latter has been widely used because it does not significantly affect subsequent TBM excavation. Furthermore, geological results can be obtained rapidly, which is crucial for construction progress.

Geophysical investigations include electromagnetic (Mahrer and List 1995), electrical (Denis et al. 2002; Ryu et al. 2011; Liu et al. 2020a), and seismic (Ashida 2001; Sattel et al. 1996; Jetschny et al. 2011; Liu et al. 2017) methods. Seismic prospecting is sensitive to fractured zones and lithological interfaces, so it is suitable for detecting tectonic differences (Liu et al. 2018a). Furthermore, the structures of most TBMs are good metallic conductors, which can adversely affect electromagnetic detection methods; seismic methods avoid this problem.

Seismic prospecting methods employ different sources to produce elastic waves and geophones coupled to the tunnel sidewall to record reflected signals. These results are then analyzed to obtain an image of the geological conditions ahead of the tunnel face. These techniques either use conventional seismic sources or the cutting motion of the cutter head as the signal source. For conventional seismic methods, active sources, such as explosives or hammers, produce the seismic waves. These sources produce relatively weak reflection signals with a wide frequency band. To limit interference from drilling activities, these conventional seismic surveys are usually conducted during maintenance work.

In recent years, a new class of seismic prospecting techniques, named tunnel seismic while drilling (TSWD) has been developed. This method can adapt to complex construction environments and the rapid tunneling of

TBM tunnels. This method uses elastic waves that are generated by the cutter head during excavation instead of traditional active sources (Petronio and Poletto 2002). Petronio and Poletto (2002) demonstrated that the TSWD method provides interpretable seismic data by cross-correlation of the pilot signal. Previously, the observation system for the TSWD method uses geophones mounted on the ground surface or tunnel entrance (Petronio et al. 2007). For deep and/or long tunnels, a pilot sensor was set on the TBM and geophones were placed along the bored tunnel.

The subject of our case study is the Gaoligongshan Tunnel, located in the Yunnan Province of China. Tunneling in this region is hazardous because fold structures are widely distributed and fractured zones are well developed. Here, a pilot tunnel precedes the main tunnel to obtain advance information as a reference for the excavation of the main tunnel. Recent results from the pilot tunnel had indicated a wide fracture zone ahead of the tunnel face, between 20 and 100 m thick, basically consistent with preliminary site investigations. We therefore chose to employ seismic methods to prospect the geological conditions, considering that faults and fracture zones are well developed in this area. We combined two different seismic methods, with complementary advantages in terms of detection distance, and considered the imaging results comprehensively. The TSWD method was used when TBM tunneling was in progress, and an active seismic source was used during maintenance; this ensured that there was no delay to the schedule.

The objective was to combine the two seismic prospecting methods to predict weathering fracture zones for the Gaoligongshan Tunnel project. These predictions could then be used to guide construction, allowing the TBM to pass safely through the fractured zones. Following successful excavation results, we used numerical simulations to develop a model to analyze the effect of the pilot tunnel on the imaging results. These results could help to prevent accidents in potentially hazardous tunnel sections.

## Background of the study area

The Gaoligongshan Tunnel is located at the western edge of the Yunnan Plateau. It is relatively long (34.5 km) and deep (maximum burial depth of 1155 m), under the southern flank of Gaoligongshan Mountain (Fig. 1). Its construction is part of the Da-Rui railway project, which stretches from Dali station to Ruili station, and it is a substantial part of the China-Myanmar international railway in Southwest China. Geographically, it is situated at the junction of the Indian and Eurasian plates. The

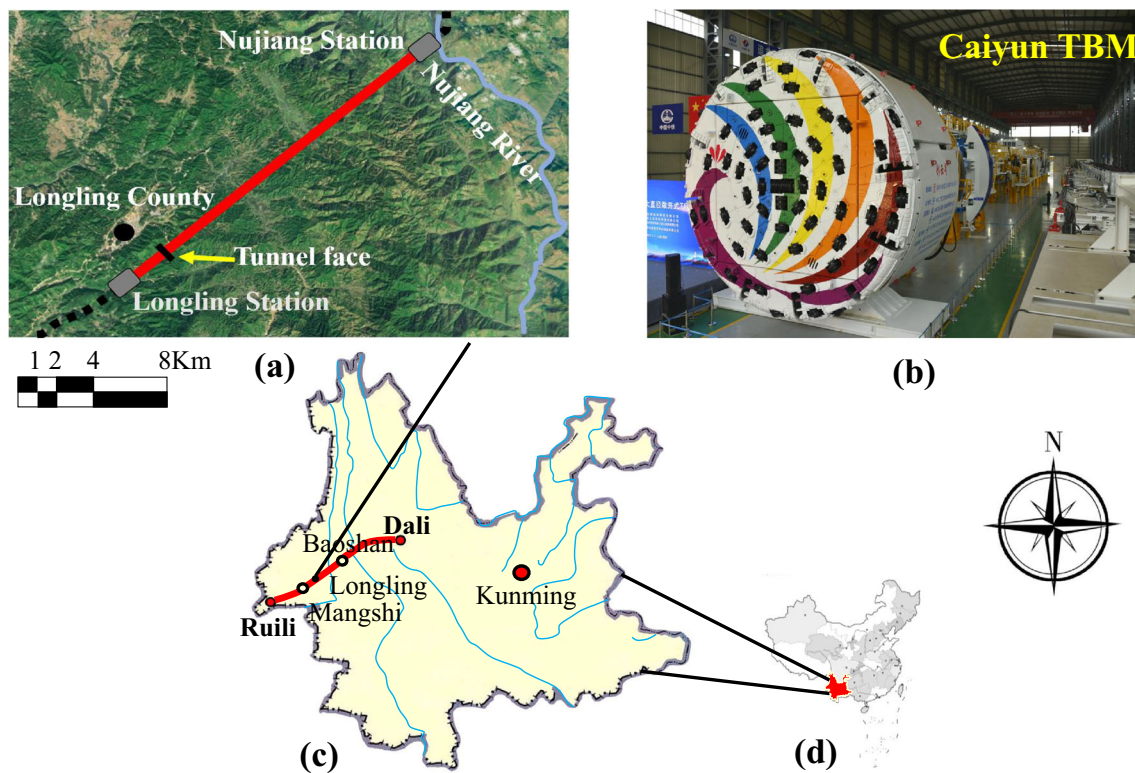


**Fig. 1** Engineering overview of the Gaoligongshan Tunnel. **a** Location overview from Google Maps. **b** The TBM used in this project (photo from the China Railway Engineering Equipment Group Co., Ltd.). **c** The location of the Da-Rui railway project. **d** The location of Yunnan Province in China

geology of this area is characterized by high geothermal energy, large ground stresses, and strong earthquakes. The construction of this tunnel is therefore particularly hazardous, so a pilot tunnel was constructed in advance of and parallel to the main tunnel to obtain reference information. Laterally, the pilot tunnel is approximately 30 m from the main tunnel, and both tunnel faces are 200 m deep. Two open TBMs with diameters of 6.39 m and 9 m were used to drill the pilot and main tunnels, respectively. This work began in 2017.

Excavation results and on-site conditions are shown in Fig. 2. The main tunnel mileage is at 224 + 386, and the pilot tunnel is slightly ahead of the main tunnel, with mileage 224 + 316 (Fig. 2d). As of July 10, 2018, 2460 m of the main tunnel had been excavated. The bedrock comprises Yanshanian granites and metamorphic rocks. Joints and fractures in the surrounding rock are well developed, and local fall-blocks can be observed. A preliminary site investigation had indicated a wide fractured zone in front of the tunnel face, approximately 20–100 m thick. However, there may be deviations in the actual position of the zone, so further detection is required. A longitudinal diagram of the tunnel, including the position of the expectant fractured zones, is shown in Fig. 2a. This information, along with photographs of the tunnel face, suggested that the quality of the rock ahead of the main tunnel was worse than expected. There is thus certain risk to the TBM as it passes

through this area, including the possibility of machine blockages and tunnel collapse.

## Methodology

### Forward prospecting schedule

The pilot tunnel was used to supplement the available information and mitigate the hazardous geological conditions while crossing the weak stratum. Additionally, we used the active seismic and TSWD methods to predict the geological condition prior to TBM excavation. The TSWD method employed pilot sensors and geophones to collect signals generated by the TBM cutter head during excavation and rock crushing, an efficient technique in deep and long tunnels. The active seismic data were collected during TBM maintenance, using a hammer source and geophones. By combining these methods, project delays were avoided by making full use of the TBM tunneling routine. The two methods are also complementary in that the TSWD method uses a lower frequency and higher energy, making it suitable for relatively long-distance detection, while the active seismic method uses a higher frequency and lower energy, making it better suited for relatively short distances. This approach enhances the quality of the advance information, aiding the safe and efficient construction of the tunnel.

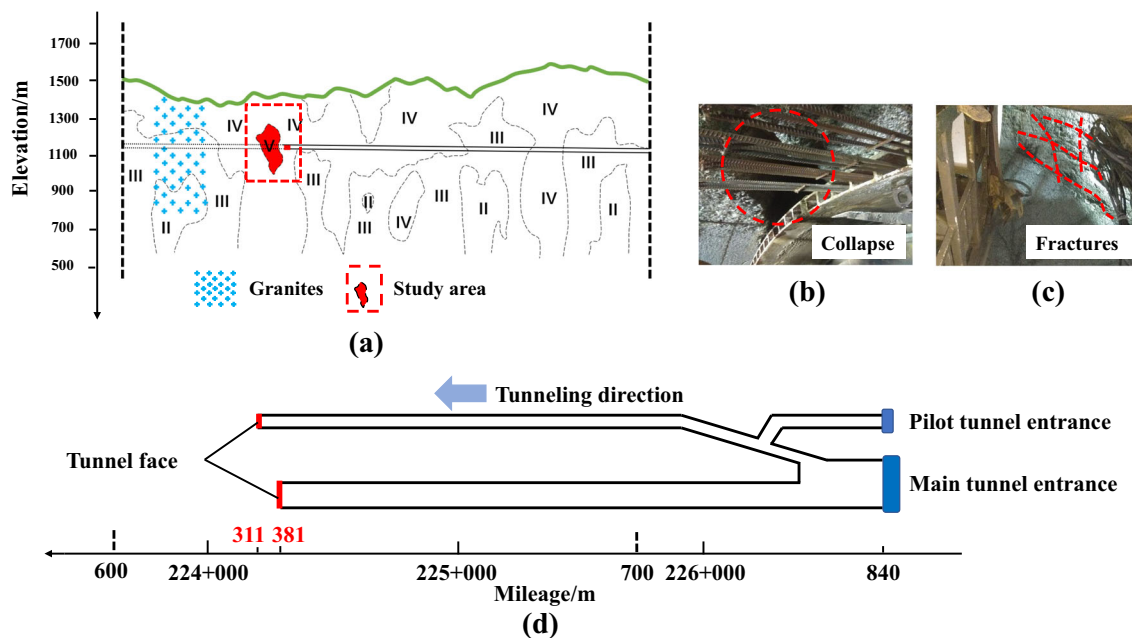


**Fig. 2** Geology surrounding the tunnel face and a schematic diagram of the tunnel. **a** The condition of the surrounding rock in the area that the tunnel is passing through, according to a preliminary geological survey (the numerals I–V indicate the grade of surrounding rock, and V refers to

the worst integrity) (the figure is modified from China Railway Eryuan Engineering Group Co., Ltd.). **b** The location of main and pilot tunnels. **c** Rock surrounding the left side of the shield. **d** Rock surrounding the right side of the shield

## TSWD method

A suitable layout of the observation system was required to obtain high-quality data from seismic wave prospecting (Liu et al. 2018b). To simplify the process of laying out the geophones, we used a different arrangement than is typically employed (Petronio et al. 2007), shown in Fig. 3. The pilot sensors (A0) were coupled close to the TBM cutter head, mainly to record the signals from cutting the rock masses while drilling. Other geophones (A1–A4, A5–A8) were installed in a straight line on the side walls behind the cutter head to record data including noise and reflections from geologic interfaces ahead of the tunnel. The geophones were spaced 3 m apart, and the minimum distance between geophone A1 and the tunnel face was 14 m. The source, the TBM cutter head, was considered to be stationary because the distance the TBM advanced during the acquisition time (a few tens of centimeters) was considerably shorter than the resolution of the  $\lambda/4$  criterion of 10–14 m (Widess 1973; Petronio et al. 2007).

The original data were recorded for approximately 20 min using the pilot sensor and geophones while the TBM was in operation at tunnel mileage 224 + 386 on July 10, 2018. We processed the data according to the steps listed in Table 1, analyzed the main effective signals, and designed a processing program to image reflector planes using the equi-travel time plane (Ashida 2001). Figure 5c and d shows cross-correlation data from the TSWD method and the results of our data processing.

The data processing comprises preprocessing and processing phases. During preprocessing, the files were formatted, the direct component (DC) was eliminated, and integral transformations were performed to establish the foundation data for subsequent calculations and analysis. To reduce the effect of random noise, we divided the data into several fragments and stacked them; stacking reduces noise and enhances data coherence. Furthermore, we used one-bit normalization, where the signal is set to 1 or –1 depending on the original sign, to normalize the waveform (Shapiro and Campillo 2004). This suppresses noise, eliminates differences between the sensors, and improves the signal-to-noise ratio (SNR) (Bensen et al. 2007).

An important step in the formal processing phase was cross-correlation because ambient construction noise could easily overwhelm the useful signals (Petronio et al. 2007). Noise sources such as the jumbolter, belt conveyor, and other machines could seriously interfere with valid signals recorded by geophones; we used cross-correlation to extract the useful signals. This helped to enhance signals and noise that were shared by two sequences (Poletto and Petronio 2006). After cross-correlation, we rebuilt the seismic recordings. The remaining steps are listed in Table 1; the same procedure was also used for the processing the traditional active seismic data.

## Active seismic prospecting method

We used the active seismic method alongside TSWD to predict geological condition ahead. The active seismic method is

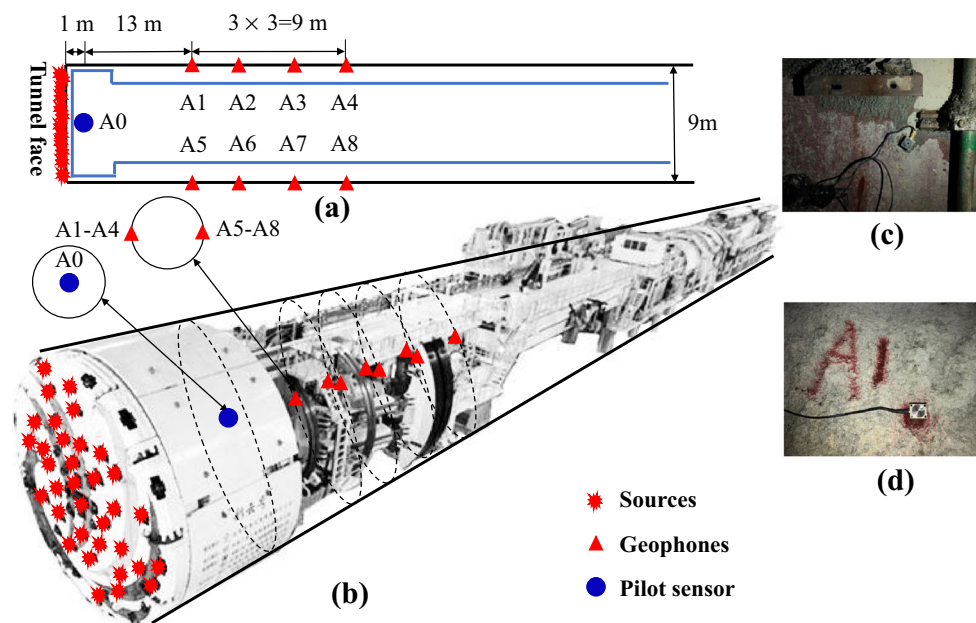


**Fig. 3** Observation system used for the TSVD method in the Gaoligongshan Tunnel. **a** Lateral view of the system. **b** Installation location of the sources, the pilot sensor, and geophones. **c** Photograph of the pilot sensor. **d** Photograph of one of the geophones

illustrated in Fig. 4. To identify the spatial position of the zones of interest, six hammer points were arranged in a circle on each side of the wall behind the face (12 points in total, S1–S12). These were struck three times to obtain high-quality data after stacking. The hammer points were spaced approximately 1 m apart, and the minimum distance between the source (S1) and the tunnel face was 13 m. Eight geophones (A1–A8) were coupled with the side wall behind the hammer points to receive reflection data from multiple directions, which improved the quality of the imaging results. The geophones were spaced 3 m apart and arranged in straight lines on either side of the tunnel. The minimum distance between geophones A1 and A5 and the tunnel face was 23 m. Figure 5a and b shows the original data and the result of our data processing. The processed results are roughly consistent with the results of the TSVD method.

The original active method data were recorded when the TBM was tunneling at mileage 224 + 381 on July 11, 2018. The TBM had progressed 5 m from the previous day when the TSVD method was employed. The data processing was divided into preprocessing and processing phases. During the preprocessing phase, the files were formatted, the DC was eliminated, and integral transformations were performed to remove low-quality data and correct differences in the amplitude between the detectors. During the processing phase, we selected direct arrivals to provide a basis for migration imaging and subsequently removed the direct waves. After a spectral analysis, band-pass filtering was used to remove some of the interference. Deconvolution was then applied to compress the length of wavelet and increase the resolution. We then

used f-k filtering to eliminate useless signals and enhance the SNR of deconvolution results (Liu et al. 2017). Finally, we used the equi-travel time plane to generate an image of the geological conditions ahead of the tunnel face (Ashida 2001).

## Results and analysis

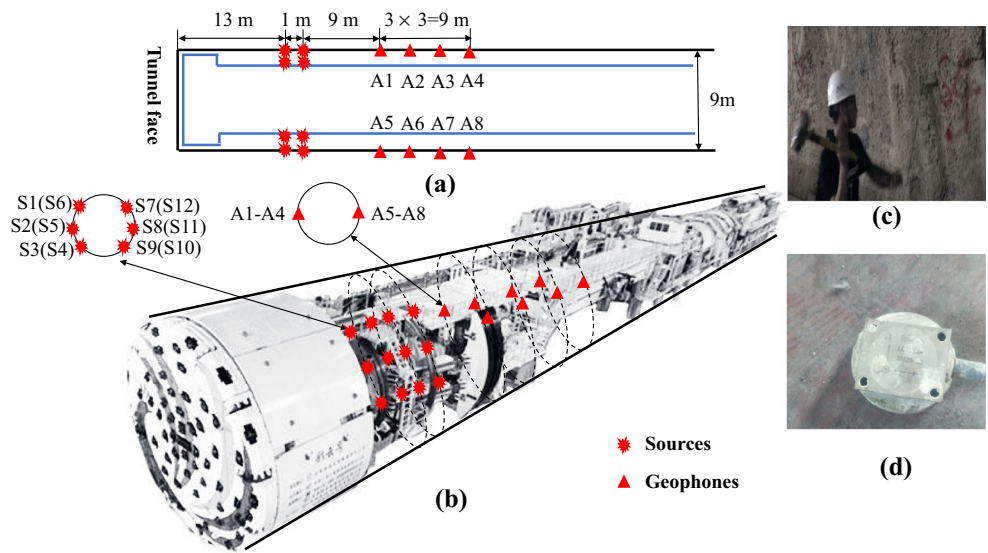
### Detection results

As described in the section “Methodology,” we derived imaging results ahead of the tunnel face from the TSVD and active seismic methods (Figs. 6 and 7). Combined with

**Table 1** Processing flow for the TSVD method with Caiyun TBM

Preprocessing	
1.	File formatting, DC elimination, data transformation
2.	Data divided into several sections and stacked
3.	1-bit processing
4.	Cross-correlation with pilot signal
Processing	
5.	Band-pass filtering
6.	Direct-arrivals picking
7.	Direct wave removal
8.	Deconvolution
9.	Wave field separation (f-k filter)
10.	Migration (equi-travel time plane)

**Fig. 4** Observation system used for the active seismic method in the Gaoligongshan Tunnel. **a** Lateral view of the system. **b** Installation locations. **c** Source points. **d** Geophones



geological analysis, areas with clear positive or negative reflections in these figures represent an interface of a fractured zone.

Between 224 + 356 and 224 + 326 and between 224 + 315 and 224 + 285, however, two distinct reflection arches can be observed. Fracture zones in the surrounding rock may therefore be discovered in this area. Additionally, between 224 + 272 and 224 + 250 and between 224 + 220 and 224 + 195, two weaker reflection zones indicate smaller fracture zones. In the regions between 224 + 286 and 224 + 272, 224 + 246 and 224 + 220, and 224 + 250 and 224 + 220, no obvious centralized reflections are visible. However, this is not clear evidence that there are no microfractures in these sections.

Similar results were obtained using the active seismic method, although there are some small distinctions. Between 224 + 356 and 224 + 328 and between 224 + 296 and 224 + 268, there are two clear reflection zones, indicating two fractured zones in these areas. Other areas exhibit relatively inconspicuous reflections, potentially indicating abnormal structures. The imaging results and a geological interpretation for the two methods are listed in Tables 2 and 3.

Along with these results, detailed geological engineering reports and maps, as well as daily site reports, were examined. Previous geological studies report that the rock surrounding the tunnel face is rated IV, and that a large fractured zone may be encountered after tunneling a further 50 m. The

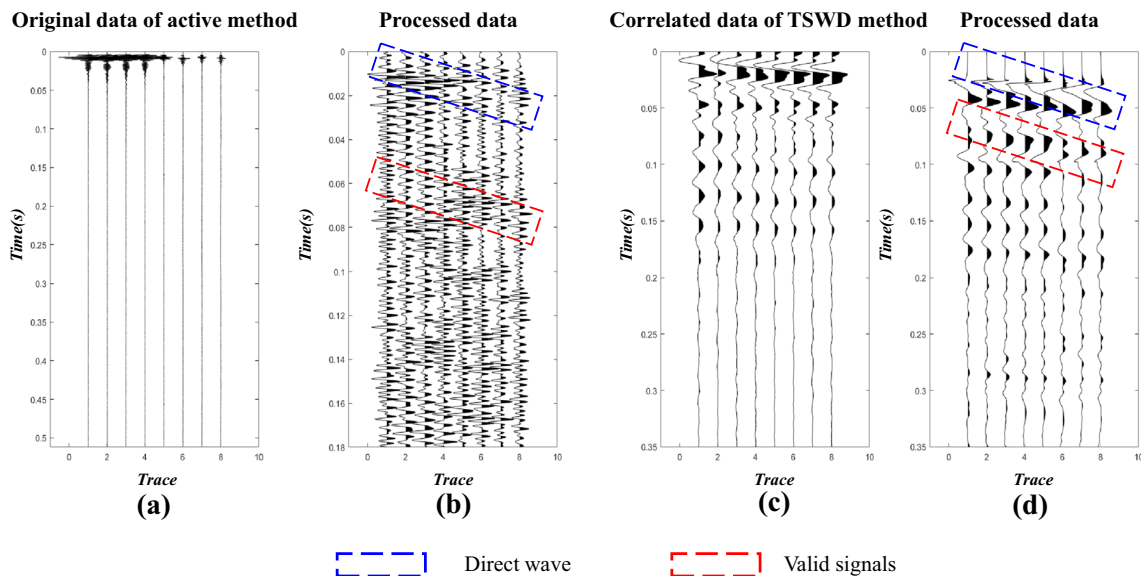


**Fig. 5** **a** Original data collected using the active method and **b** correlated data of the TSWD method and their processed results (**c**, **d**)

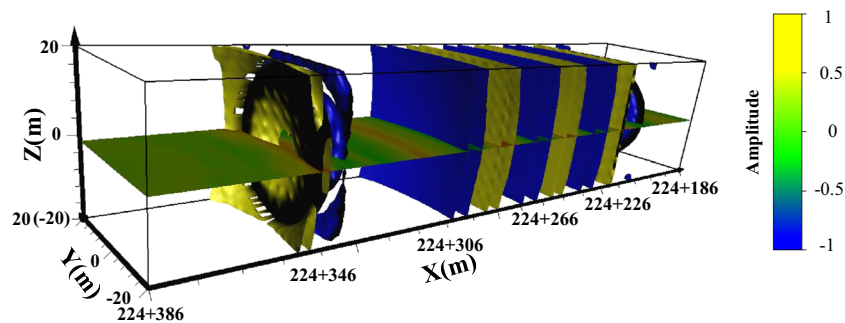


**Fig. 6** Imaging results from the TSWD method. Investigation depth is approximately 200 m, the  $x$ -axis is the tunnel axis, the  $y$ -axis is parallel to the bottom of the tunnel, and the  $z$ -axis is perpendicular to the bottom of tunnel

surrounding rock in this area is rated V (Fig. 2). A fractured zone, joints, fracture development, and local fall-blocks were observed in the rocks surrounding the tunnel face. There is no clear indication that the quality of the rock ahead of the tunnel face will improve, in agreement with the preliminary geological survey (Fig. 2).

These observations and the imaging results of both survey methods together indicate that (a) there is a high probability that there are two fractured zones at approximately 224 + 350 and 224 + 310 ahead of the tunnel face, and (b) the rock mass elsewhere appears to be of poor integrity.

### Recommendations for tunneling construction

The interpretation of the imaging results and geological reports suggests that the predicted fractured zone could have a negative impact on the TBM tunneling, and that there are security risks associated with crossing this area, including machine blockage and tunnel collapse. Reasonable measures, such as adjusting the driving scheme and strengthening the support mechanisms, should be taken to ensure safety.

As such, we have made the following recommendations to the construction company:

- Reduce tunneling speed because of poor integrity of the rock ahead of the tunnel face.

- Employ concrete reinforcements in the tunnel section where the fragmented zone of the fault is expected. This can prevent or reduce the deformation of the surrounding rock.
- Upgrade/strengthen the tunnel supports by erecting more steel arches (reducing the spacing to 90 cm), laying mesh reinforcement (to prevent falling rock), and spraying concrete onto the fragmented zone, while tunneling in the area where the fractured zone is predicted. This should reduce the duration that the surrounding rock is exposed, and will form a stable support system.

### Result validation

In line with our predictions, the range of weathering and fracture zones was encountered during subsequent tunnel excavation. The construction company had upgraded the tunnel support system based on our recommendations, and no major incidents occurred as the TBM passed through the area. Once the excavation of this area was complete, a geological sketch map for the main tunnel in the positive direction of the tunnel-axis was created. This map was compared to the imaging results of the two methods, as shown in Fig. 8.

There were several fall-block areas and a collapse area (2 m × 4 m) at 224 + 370 and 224 + 355, respectively; corresponding

**Fig. 7** Imaging results from the active seismic method. Investigation depth is approximately 130 m, the  $x$ -axis is the tunnel axis, the  $y$ -axis is parallel to the bottom of the tunnel, and the  $z$ -axis is perpendicular to the bottom of tunnel

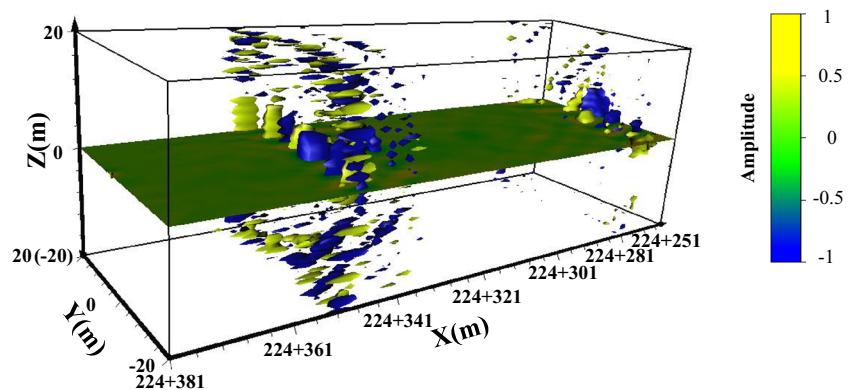


**Table 2** Imaging results and geological interpretation using the TSWD method

Position	Imaging results	Geological interpretation
224+356–224+326	Large-scale distinct reflection arc	Fault-affected zone 30 m wide or a distinct geological interface with collapse
224+315–224+285	Wide anomalous zone	Weathered zone in surrounding rock with poor integrity
224+272–224+250	Small anomalous zone	Fractured zone with poor integrity
224+220–224+195	Anomalous zone	Weathered zone

photographs are shown in Fig. 9a and b. However, the volume of these geologic bodies was so small that they were not observed in our imaging results. Between 224 + 350 and 224 + 330, fractured zones were the major geological features (Fig. 8c). These coincide with the positions of the clear reflections shown in the imaging results (Fig. 8a and b). Between 224 + 325 and 224 + 290, a similar fractured zone was described by the map (Figs. 8c and 9c). The imaging survey results indicate a reflection in this region, but there is a discrepancy between the actual position and the predicted position, with the latter being further back. Furthermore, while tunneling at 224 + 250, a fracture was found running through the dome (Fig. 9d).

There are a number of possible causes of these discrepancies. First, the pilot tunnel has a certain impact on the final images, particularly for the data collected by the geophones on the wall closest to the pilot tunnel. Some of the energy from the source may propagate between the main tunnel and the pilot tunnel several times, which would disrupt the waves and interfere with the resulting image if it is not taken into account. Another possible cause is the low dominant TSWD signal frequency (60–90 Hz), which may have resulted in a resolution that was insufficient to detect the narrow gap between the interfaces. Furthermore, artificial interference from environmental factors at the site during the process of active seismic prospecting may have caused inaccuracies.

## Discussion

Following the analyses of the survey results, we determined that the SNR of the signals recorded by the geophones and the quality of the imaging results were affected by the pilot tunnel. To quantify the effect of the advance pilot tunnel, a numerical simulation was employed to model seismic records for different situations. These included models both with and without a pilot tunnel, as well as different sources and geophone

positions for the TSWD and active seismic methods. Appropriate analyses were then performed to identify techniques to guide practical detection work in the future and produce more accurate predictions for projects with an advance pilot tunnel.

## Numerical simulation methods

The two-dimensional finite difference time domain (2D FDTD) method with absorbing boundary conditions was employed. On the basis of the excavation results, we established a model for our numerical simulation (Fig. 10a and b), measuring 200 m and 100 m in the  $x$  and  $y$  directions, respectively. The relative positions and diameters of the main and pilot tunnels were based on the Gaoligongshan project. Three abnormal areas with low seismic velocities were included in our model. These areas were 15 m, 30 m, and 5 m wide and were based on the geological record after excavation. The velocities of the different areas in the model are shown in Fig. 10d. For clarity, we have denoted the side of the main tunnel furthest from the pilot tunnel as the left side, and the side closer to the pilot tunnel as the right side.

## Simulation of the active seismic method

The observation setup for the active seismic method is shown in Fig. 10b. To record more reflection data, we installed twenty geophones on both walls at 2-m intervals. The geophones were arranged in a straight line with A1–A20 on the left wall and with A21–A40 on the right wall. The distance between the source point and the tunnel face was 45 m (Fig. 10b). A 400-Hz Ricker wavelet was used as the source for the numerical model because the master frequency of the actual test source was approximately 400 Hz (Fig. 11b).

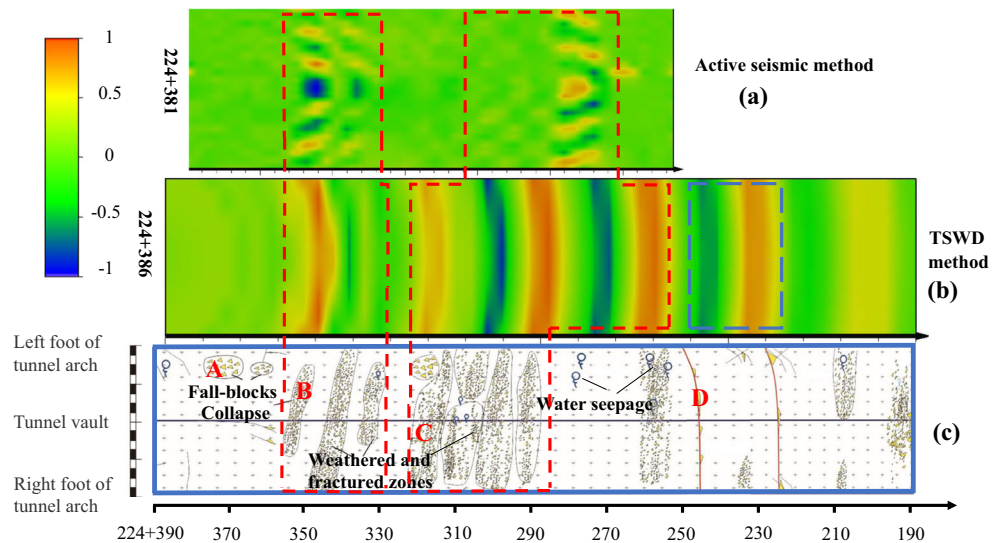
To assess the effect of the pilot tunnel on the seismic data, two additional models without abnormal zones, one with a

**Table 3** Imaging results and geological interpretation using the active seismic method

Position	Imaging results	Geological interpretation
224+356–224+330	Clear and serried reflection zone	Fractured zone with extremely broken surrounding rock
224+296–224+268	Weaker reflection zone	Weathered zone with poor surrounding rock



**Fig. 8** Comparison of the TSWD and active seismic imaging results with the geological feature sketch map after tunneling. **a** Imaging result for the active seismic method with a detection range between 224 + 381 and 224 + 251. **b** Imaging result for the TSWD method with a detection range between 224 + 386 and 224 + 186. **c** Sketch map of geological features between 224 + 390 and 224 + 186 after tunneling (the red letters A, B, C, and D refer to the location of typical geological conditions, which correspond to Fig. 9a, b, c, and d, respectively)



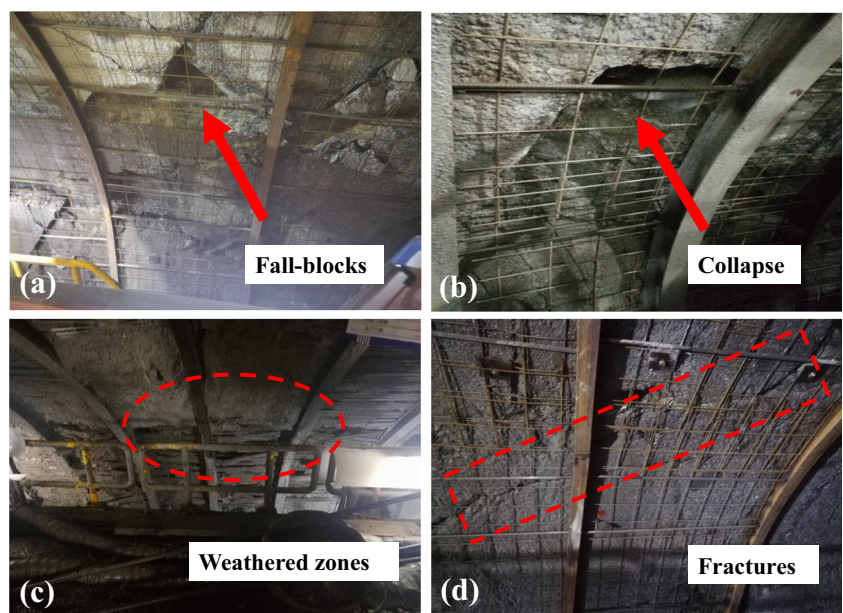
pilot and a main tunnel and the other with only a pilot tunnel, were used in the forward modeling program (Fig. 12a and d). These models had velocities approximately equal to the first model. From these, we obtained the interference wave produced by the pilot tunnel, which was then used to determine the effective signals from the fractured zones by subtraction (Fig. 12). The effect of the abnormal zones on the seismic data was similarly determined. The data from the model with only the tunnel and pilot tunnel were subtracted from the data from the model with the tunnel, pilot tunnel, and abnormal zones. The maximum amplitude was extracted for every trace in these recordings, so that they could be used as reference amplitudes for such signals (Fig. 13).

In subsequent recordings, we removed the interference from the original data to isolate the data from the abnormal

zones for analysis. When the source was on the left wall, the arrival time of the reflection from the fractured zone was clearly recorded by the sensors on the left wall. The amplitude of the effective signals from the fractured zones is much larger than the amplitude of the interference wave produced by the pilot tunnel (Fig. 13a). Thus, the pilot tunnel has little impact on the quality of the original data under these conditions. The data from the right wall indicate that the wave from the fractured zone and the interference wave are distinct. It was thus possible to filter out the interference signal with the tau-p filtering method. The results are shown in Fig. 14c.

When the source was set on the right wall, we observed clear reflections from the fractured zone at 0.05 s, 0.07 s, and 0.1 s (Fig. 15). The amplitude of the signal from the fractured zone was again greater than the amplitude of the interference

**Fig. 9** Geological conditions after tunneling through the study area. **a** Fall-blocks at 224 + 370. **b** Collapse at 224 + 370. **c** Weathered zone between 224 + 350 and 224 + 330. **d** Fractures at 224 + 325



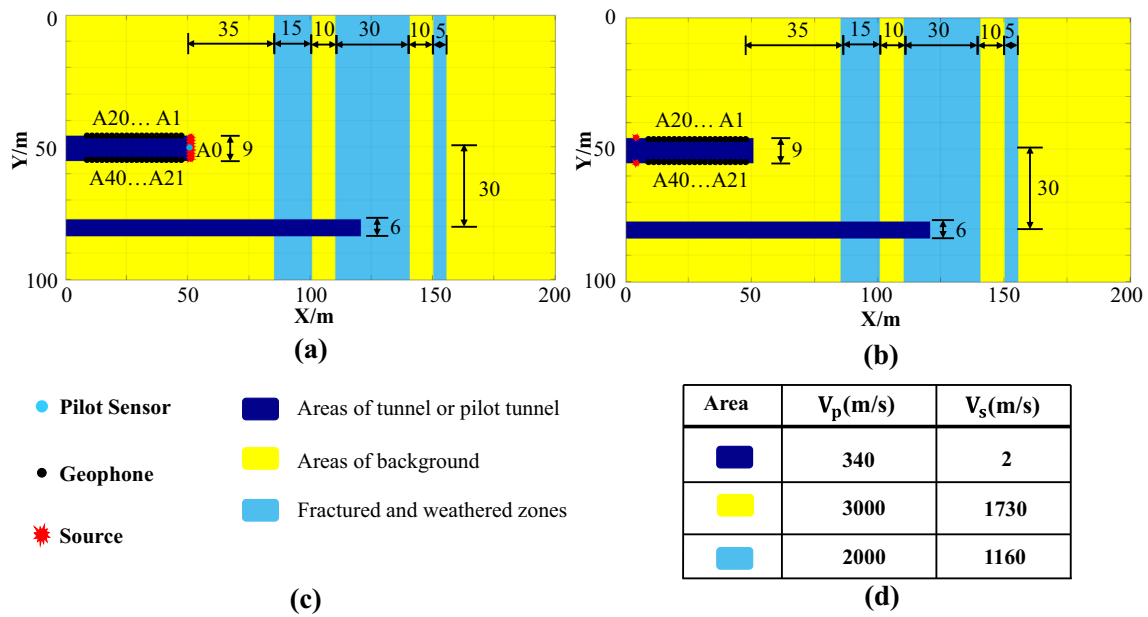


**Fig. 10** Geological models for a numerical simulation based on the actual excavation results. **a** Model of the TSWD method. **b** Model of the active seismic method. **c** Interpretation of the geological models. **d** The velocities of shear wave and compression wave in the models

wave (Fig. 13c). The data from the sensors on the right wall indicated that the interference signal was nearly hyperbolic, but with a different direction than when the source was set up on the left wall, which was caused by the different positions of the source (Fig. 15b). Furthermore, although there was significant wave propagation in the rock between the main tunnel and the pilot tunnel, the waves could be obstructed as reflections repeatedly oscillated between the main tunnel and the pilot tunnel. This process could obscure the signal from the

fractured zone such that it could no longer be extracted (Fig. 15b).

**Simulation of the TSWD method**

The data recording for the TSWD method is shown in Fig. 10a. Geophone placement was the same as for the simulations of the active seismic method. An additional pilot sensor (A0) was placed on the center of the tunnel face. Unlike

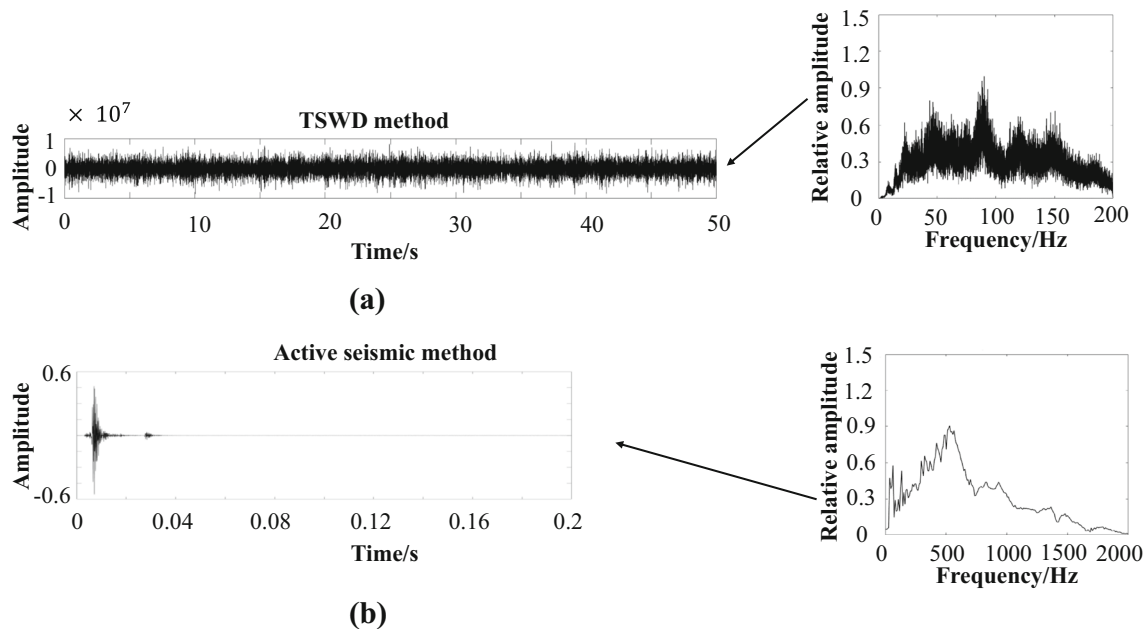


**Fig. 11** Source signals for the numerical model. **a** Pilot signals with frequency spectrum, recorded during the field test and used as a source signal. **b** Signals from the active seismic method with frequency spectrum recorded during the field test

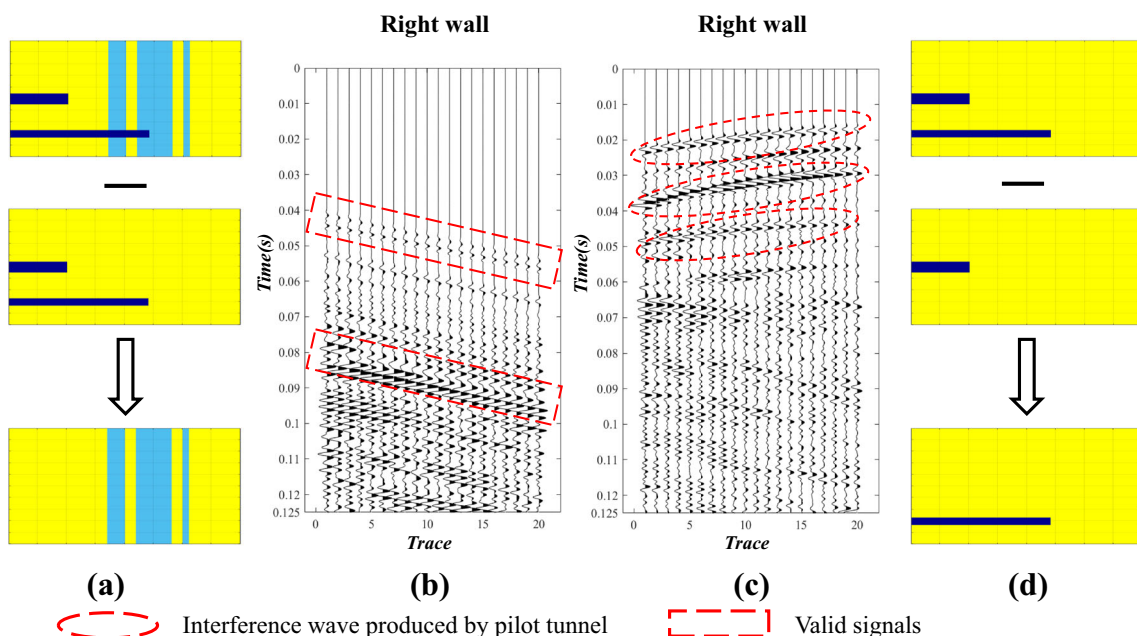


**Fig. 12** Process of obtaining interference and primary signals. **a** Obtaining the primary signals. **b** Primary signals from the recording on the right wall with the source point on the right wall. **c** Interference signals

from the recording on the right wall with the source point on the right wall. **d** Obtaining the interference signals

the active seismic method, the source points were combined with the tunnel face. To simulate the TSWD method realistically, the pilot signals that were recorded in the field test, shown in Fig. 11a, were employed as the sources for the simulation. To simulate multiple cutters working together, we

deployed sources every 2 m along the tunnel face, resulting in continuous, disordered signals.

The simulation results (Fig. 16) were used to illustrate differences in data recorded by the sensors on either side of the tunnel. The geophones placed on the left wall (Fig. 16c)

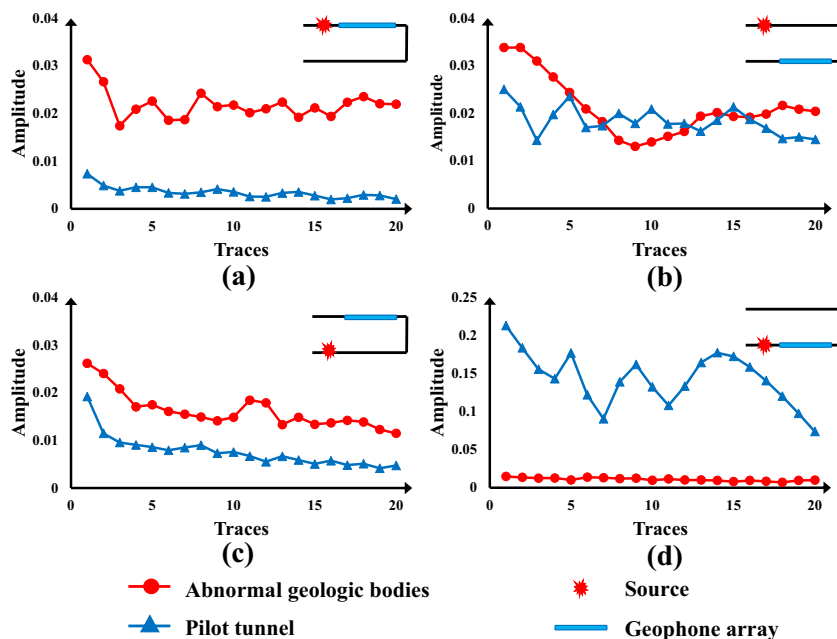


**Fig. 13** Comparison of the amplitude under different conditions. Amplitude of the interference and primary signals when **a** the source point is on the left wall and the geophones are on the left wall, **b** the source point is on the left wall and the geophones are on the right wall, **c**

the source point is on the right wall and the geophones are on the left wall, and **d** the source point is on the right wall and the geophones are on the right wall

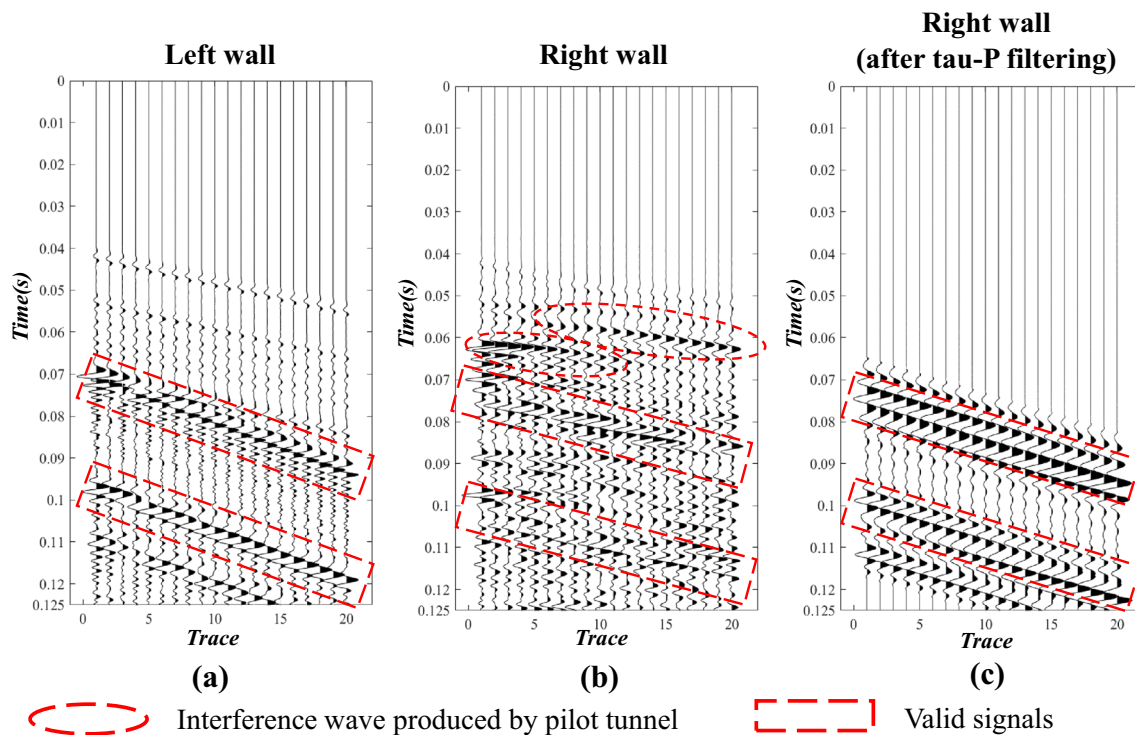


**Fig. 14** Numerical simulation results for the active seismic method with the source point on the left wall. Recording from **a** the left wall, **b** the right wall, and **c** the right wall after tau-p filtering

clearly recorded waves reflected by the fractured zone, allowing the interface to be outlined based on their arrival time and the background velocity.

In contrast, the geophones on the right wall (Fig. 16d) recorded many fragments of hyperbolic seismic events, in addition to

reflections of the primary wave between the main tunnel and the pilot tunnel. These hyperbolic events were made clearer by subtracting the primary wave (Fig. 16d). Interestingly, we were unable to completely *subtract* the primary wave at 0.01 s (Fig. 16a and c). This could be a result of influence from the

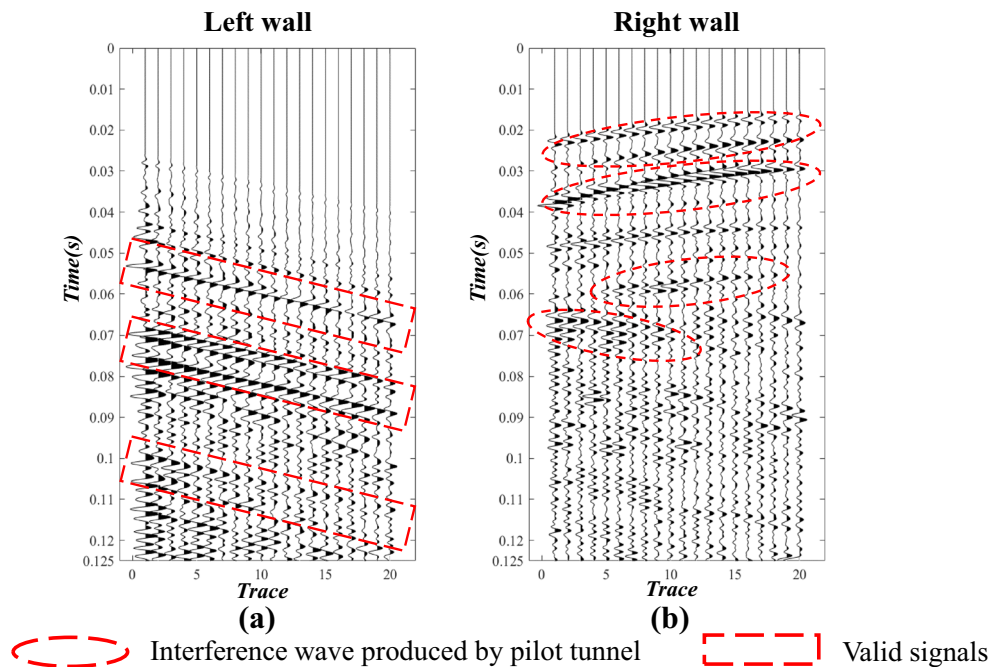


**Fig. 15** Numerical simulation results for the active seismic method with the source point on the right wall. Recording from **a** the left wall and **b** the right wall

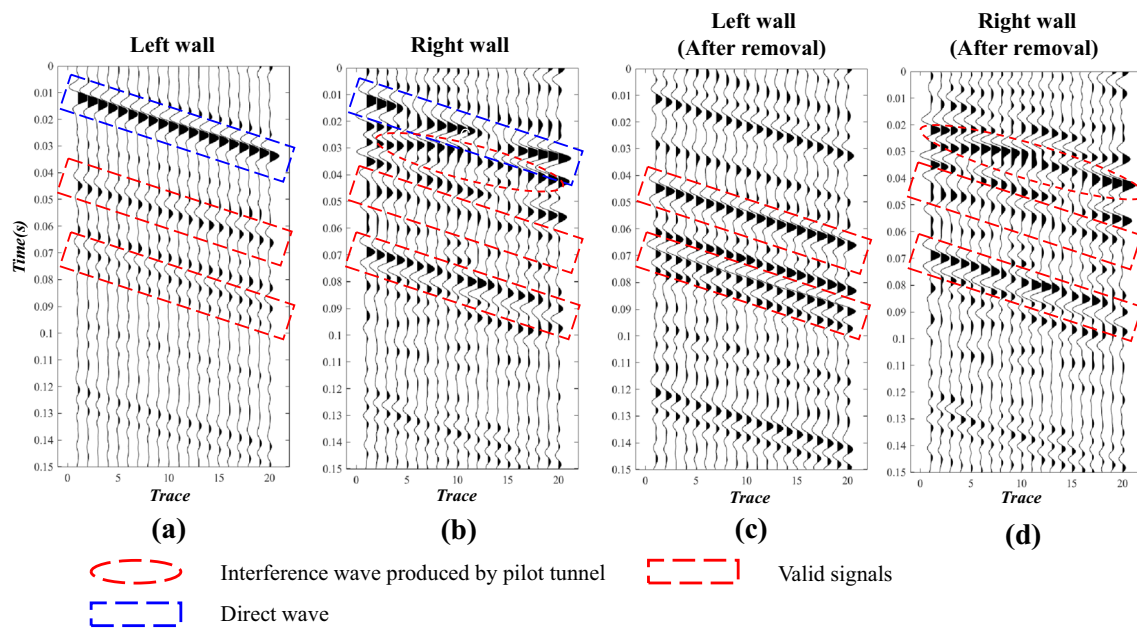


**Fig. 16** TSWD numerical simulation results. Original recordings from **a** the left wall and **b** the right wall. Recording after removing the primary wave for **c** the left wall and **d** the right wall

cross-correlation operation. Additionally, the amplitudes of the primary wave and the interference wave were approximately the same after cross-correlation and were similar to the recording in Fig. 14b. Hence, the same method, tau-p filtering, was employed to remove the interference wave.

### Summary of simulation results

For the active seismic method, our results demonstrate that seismic recordings from the left wall mirrored the vertical fault zone interfaces, independent of the source location. When the sources were set on the left wall, the wave reflected by the fault zone was quite clear and the effect of the pilot tunnel was minimal, resulting in a comparatively accurate image. The signal recorded from the right wall, however, was relatively poor, as a result of interference from the pilot tunnel. The effect was even worse when the source was on the right of the tunnel face. For the TSWD method, the recording from the left wall was fairly clear after cross-correlation, while the recording from the right wall required tau-p filtering to remove the interference wave. This may be an effective method, but it has not been confirmed using field data.

To provide more accurate prospecting results and prevent accidents or complications that result in expensive standstills, therefore, source points could be set up on the left wall to minimize the effect of an interference wave. Furthermore, more geophones should be employed on the left wall to collect more data with a higher SNR, while relatively fewer geophones should be positioned on the right wall to limit interference from the pilot tunnel. If the spatial position of geological interfaces must be determined, a large number of geophones on both walls should

be used. Additionally, for data collected from the right wall, tau-p filtering, or other filtering techniques, during processing will yield more accurate results.

### Resolution evaluation

The TSWD method and the active seismic method are based on the principle of elastic waves, similar to seismic tomography technology (Shang et al. 2018). The primary difference between the two methods is the master frequency, and hence a different resolution. Generally we use 1/4 wavelength as the theoretical resolution. As mentioned above, the dominant TSWD signal frequency is 60–90 Hz, and the resolution in theory is 5.6–8.3 m at a seismic velocity of 2000 m/s. For the active seismic method, the master frequency is 400 Hz and the resolution in theory is 1.25 m. Both methods can detect and locate a single discontinuity. For rock joints (Shang et al. 2012) that are concentrated and widely distributed over a certain region, the position of an abnormal body can be determined with this method. If there are two interfaces, both at a distance between 1 and 5 m, the active source method can detect both interfaces in theory, while TSWD can only detect one. Thus, interfaces can be more comprehensively detected by applying both the active seismic and TSWD methods together.

### Conclusion

Building deep, long tunnels, or tunneling in mountainous terrain, with TBMs remains challenging. Machine blockages and

tunnel collapse events are persistent threats. Using combined seismic prospecting methods would help engineers mitigate some of these hazards. In this study, TSWD and active seismic methods were used in combination to predict geological conditions during tunnel construction. Two large fractured zones were successfully predicted with the technique. On the basis of recommendations made from our data, the Caiyun TBM successfully tunneled through the two areas.

The influence of a pilot tunnel on seismic signals was investigated with numerical simulations. The results demonstrated that geophones on the tunnel wall further from the pilot tunnel receive clear primary signals, while geophones on the wall nearer the pilot tunnel received more interference created by the pilot tunnel. While designing an observation system, more geophones should thus be coupled to the far wall than on the near wall. Additionally, the active seismic source should also be positioned on the wall further from the pilot tunnel. It is necessary to verify this proposed improved observation system with data from post-excavation studies in the future. Furthermore, advanced methods such as reverse time migration and deep-learning inversion can also be used to improve detection quality in the future studies (Li et al. 2020; Liu et al. 2020b).

**Acknowledgements** The authors thank the Yungui Railway Yunnan Co., Ltd., China Railway Tunnel Group and the China Railway Engineering Equipment Group Co., Ltd. for their contributions and assistance in the publication of this paper.

**Funding** This work was supported by the National Natural Science Foundation of China under Grant numbers 51739007, U1806226, 51922067 and 51809155, the National Key Research and Development Plan under Grant number 2016YFC0801604.

## References

- Ashida Y (2001) Seismic imaging ahead of a tunnel face with three-component geophones. *Int J Rock Mech Min Sci* 38(6):823–831. [https://doi.org/10.1016/S1365-1609\(01\)00047-8](https://doi.org/10.1016/S1365-1609(01)00047-8)
- Barton N (2012) Reducing risk in long deep tunnels by using TBM and drill-and-blast methods in the same project—the hybrid solution. *J Rock Mech Geotech Eng* 4(2):115–126. <https://doi.org/10.3724/SP.J.1235.2012.00115>
- Bensen GD, Ritzwoller MH, Barmin MP, Levshin AL, Lin F, Moschetti MP, Yang Y (2007) Processing seismic ambient noise data to obtain reliable broad-band surface wave dispersion measurements. *Geophys J Int* 169(3):1239–1260. <https://doi.org/10.1111/j.1365-246X.2007.03374.x>
- Chen G, Wu ZZ, Wang FJ, Ma YL (2011) Study on the application of a comprehensive technique for geological prediction in tunneling. *Environ Earth Sci* 62(8):1667–1671. <https://doi.org/10.1007/s12665-010-0651-y>
- Denis A, Marache A, Obellianne T, Breyse D (2002) Electrical resistivity borehole measurements: application to an urban tunnel site. *J Appl Geophys* 50(3):319–331. [https://doi.org/10.1016/S0926-9851\(02\)00150-7](https://doi.org/10.1016/S0926-9851(02)00150-7)
- Jetschny S, Bohlen T, Kurzmann A (2011) Seismic prediction of geological structures ahead of the tunnel using tunnel surface waves. *Geophys Prospect* 59(5):934–946. <https://doi.org/10.1111/j.1365-2478.2011.00958.x>
- Jiao YY, Tian HN, Liu YZ, Mei RW, Li HB (2015) Prediction of tunneling hazardous geological zones using the active seismic approach. *Near Surface Geophysics* 13(4):333–342. <https://doi.org/10.3997/1873-0604.2015017>
- Li S, Liu B, Xu X, Nie L, Liu Z, Song J, Sun H, Chen L, Fan K (2017) An overview of ahead geological prospecting in tunneling. *Tunn Undergr Space Technol* 63:69–84. <https://doi.org/10.1016/j.tust.2016.12.011>
- Li S, Liu B, Ren Y, Chen Y, Wang Y, Jiang P (2020) Deep-learning inversion of seismic data. *IEEE Trans Geosci Remote Sens* 58(3):2135–2149. <https://doi.org/10.1109/TGRS.2019.2953473>
- Liu B, Chen L, Li S, Song J, Xu X, Li M, Nie L (2017) Three-dimensional seismic ahead-prospecting method and application in TBM tunnelling. *J Geotech Geoenviron* 143(12):04017090. [https://doi.org/10.1061/\(ASCE\)GT.1943-5606.0001785](https://doi.org/10.1061/(ASCE)GT.1943-5606.0001785)
- Liu B, Zhang F, Li S, Li Y, Xu S, Nie L, Zhang C, Zhang Q (2018a) Forward modelling and imaging of ground-penetrating radar in tunnel ahead geological prospecting. *Geophys Prospect* 66(4):784–797. <https://doi.org/10.1111/1365-2478.12613>
- Liu B, Chen L, Li S, Xu X, Liu L, Song J, Li M (2018b) A new 3D observation system designed for a seismic ahead prospecting method in tunnelling. *Bull Eng Geol Environ* 77:1547–1565. <https://doi.org/10.1007/s10064-017-1131-3>
- Liu B, Pang Y, Mao D, Wang J, Liu Z, Wang N, Liu S, Zhang X (2020a) A rapid four-dimensional resistivity data inversion method using temporal segmentation. *Geophys J Int* 221(1):586–602. <https://doi.org/10.1093/gji/ggaa019>
- Liu B, Guo Q, Li S, Liu B, Ren Y, Pang Y, Xu G, Liu L, Jiang P (2020b) Deep learning inversion of electrical resistivity data. *IEEE Trans Geosci Remote Sens* 58(8):5715–5728. <https://doi.org/10.1109/TGRS.2020.2969040>
- Mahrer KD, List DF (1995) Radio frequency electromagnetic tunnel detection and delineation at the Otay Mesa site. *Geophysics* 60(2):413–422. <https://doi.org/10.1190/1.1443778>
- Parise M, De Waele J, Gutierrez F (2008) Engineering and environmental problems in karst—an introduction. *Eng Geol* 3(99):91–94. <https://doi.org/10.1016/j.enggeo.2007.11.009>
- Petronio L, Poletto F (2002) Seismic-while-drilling by using tunnel boring machine noise. *Geophysics* 67(6):1798–1809. <https://doi.org/10.1190/1.1527080>
- Petronio L, Poletto F, Schleifer A (2007) Interface prediction ahead of the excavation front by the tunnel-seismic-while-drilling (TSWD) method. *Geophysics* 72(4):G39–G44. <https://doi.org/10.1190/1.2740712>
- Poletto F, Petronio L (2006) Seismic interferometry with a TBM source of transmitted and reflected waves. *Geophysics* 71(4):SI85–SI93. <https://doi.org/10.1190/1.2213947>
- Price DG (2008) *Engineering geology: principles and practice*. Springer Science & Business Media
- Ryu HH, Cho GC, Yang SD, Shin HK (2011) Development of tunnel electrical resistivity prospecting system and its application. *Berichte Geol. B.-A.*, 93. International Workshop on Geoelectric Monitoring 179–183. <http://hdl.handle.net/10203/171746>
- Sattel G, Sander B, Amberg F, Kashiwa T (1996) Predicting ahead of the face. *Tunnels & Tunnelling International* <http://worldcat.org/issn/0041414X>
- Shang J, Luo X, Gao F, Hu J, Zhou K (2012) Advanced predication of geological anomalous body ahead of laneway using seismic tomography technique. *Procedia Engineering* 43:324–330. <https://doi.org/10.1016/j.proeng.2012.08.056>

- Shang J, West LJ, Hencher SR, Zhao Z (2018) Geological discontinuity persistence: implications and quantification. *Eng Geol* 241:41–54. <https://doi.org/10.1016/j.enggeo.2018.05.010>
- Shapiro NM, Campillo M (2004) Emergence of broadband Rayleigh waves from correlations of the ambient seismic noise. *Geophysical Research Letters* 31(7). <https://doi.org/10.1029/2004GL019491>
- Tiantian S, Zhengxue X, Huayou SUE, Xiaoxia L (2004) Engineering geological analysis of 2• 22 blockage accident in TBM construction of Shanggongshan tunnel. *Chin J Rock Mech Eng* 23(4):544–544
- Vibert C, Gupta SC, Felix Y, Biquet J, Robert F (2005) Dul Hasti hydroelectric project (India): experience gained from back analysis of the excavation of the head race tunnel. *Proceedings of Geoloine*: 23–25. <https://doi.org/10.1016/j.proeng.2012.08.056>
- Widess MB (1973) How thin is a thin bed? *Geophysics* 38(6):1176–1180. <https://doi.org/10.1190/1.1440403>
- Yin J, Shang Y, Fu B, Qu Y (2005) Development of TBM-excavation technology and analyses & countermeasures of related engineering geological problems. *Gongcheng Dizhi Xuebao. J Eng Geol* 13(3): 389–397
- Yokota Y, Yamamoto T, Shirasagi S, Koizumi Y, Descour J, Kohlhaas M (2016) Evaluation of geological conditions ahead of TBM tunnel using wireless seismic reflector tracing system. *Tunneling and Underground Space Technology* 57:85–90. <https://doi.org/10.1016/j.tust.2016.01.020>
- Zhang J, Fu B (2007) Advances in tunnel boring machine application in China. *Yanshilixue Yu Gongcheng Xuebao. Chin J Rock Mech Eng* 26(2):226–238